Direct Simulation of Hypersonic Flows Over Blunt Wedges

Vincent Cuda Jr.*
Old Dominion University Research Foundation, Norfolk, Virginia
and
James N. Moss†
NASA Langley Research Center, Hampton, Virginia

The results of a numerical study of low-density hypersonic flow about cylindrically blunted wedges with body half-angles of 0, 5, and 10 deg are presented. Most of the transitional flow regime encountered during entry between the free molecule and continuum regimes is simulated for a re-entry velocity of 7.5 km/s by including freestream conditions of 70 to 100 km. The bodies are at zero angle of incidence and have diffuse and finite catalytic surfaces. Translational, thermodynamic, and chemical nonequilibrium effects are considered in the numerical simulation by utilizing the direct simulation Monte Carlo (DSMC) method. The numerical simulations show that noncontinuum effects such as surface temperature jump and velocity slip are evident for all cases considered. The onset of chemical dissociation occurs at a simulated altitude of 96 km for the configurations considered.

Nomenclature

A_b = base area
C_D = drag coefficient, $2F_x/\rho_\infty U_\infty{}^2 A_b$
C_H = heat transfer coefficient, $2q/\rho_\infty U_\infty^3$
C_i = mass fraction of species i, ρ_i/ρ
C_p = pressure coefficient, $2p/\rho_\infty U_\infty^2$
C^* = $\mu^* T_\infty/\mu_\infty T^*$
F = force
Kn = Knudsen number, λ/ℓ or $(\lambda/\rho)(d\rho/d\eta)$
K_r^2 = Cheng's parameter, $p_\infty R_N/\mu_\infty U_\infty C^* = \sqrt{\pi} R_N/2S_\infty \lambda_\infty C^*$
ℓ = characteristic dimension
M = Mach number
$\bar{M}$ = molecular weight of mixture
n = number density
p = pressure
q = heat flux
R = universal gas constant = 8.3143 J/mol k
R_B = base radius
R_N = nose radius
Re_∞ = Reynolds number, $\rho_\infty U_\infty R_N/\mu_\infty$
s = coordinate along body surface
S_∞ = speed ratio, $U_\infty\sqrt{\bar{M}/2RT_\infty}$
T = thermodynamic temperature
T_{ov} = overall kinetic temperature
T^* = $(T_{0,\infty} + T_w)/2$
u = velocity component tangent to body surface
U_∞ = freestream velocity
v = velocity component normal to surface
X_i = mole fraction of species i
x = coordinate measured along the body centerline
y = coordinate measured normal to the body centerline
γ = ratio of specific heats
η = coordinate normal to body surface
θ = body half-angle
λ_∞ = freestream mean free path
μ = viscosity
μ^* = viscosity evaluated at T^*
ρ = density

Subscripts

i = ith species
w = wall values
∞ = freestream values
0 = total values

Presented as Paper 86-1348 at the AIAA/ASME 4th Joint Thermophysics and Heat Transfer Conference, Boston, MA, June 2–4, 1986; received Aug. 11, 1986; revision received Dec. 4, 1986.

*Graduate Student. Member AIAA.
†Research Engineer. Associate Fellow AIAA.

Introduction

MUCH of the focus of hypersonic computational fluid dynamics during the 1970s was centered on the Shuttle program and the planetary entry programs. Among the planetary programs, the major emphasis was the Galileo probe, which is designed to penetrate into the atmosphere of Jupiter at a relative velocity of 48 km/s. Currently, we find the boundaries of this research expanding rapidly by new advanced applications[1] such as aeroassisted orbital transfer vehicles (AOTV) that achieve payload economy by passing through the Earth's upper atmosphere to change orbit; a transatmospheric vehicle (TAV) that takes off from Earth or stages from a conventional aircraft and enters near-Earth orbit, then re-enters the atmosphere with cross-range capability to land on an airstrip; and the hypersonic aircraft anticipated to require propulsion by supersonic combustion ramjets. Together, these new applications encompass a broad range of physical phenomena that present many experimental and numerical simulation challenges.

A problem common to these new applications is the nonequilibrium nature of the flow for some portion of the flight and the heating pulse. Even though peak heating and the primary maneuvering will occur under continuum conditions for most hypersonic vehicles, some portion of the vehicle may experience rarefied, transitional flow, particularly the leading edges or the nose region of the vehicle. Furthermore, the shock wave is a highly nonequilibrium region irrespective of altitude under hypersonic conditions. For the transitional hypersonic flow, the numerical simulation is complicated because there is usually an absence of equilibrium among the various energy modes—translational, internal, and chemical. If the flow is sufficiently energetic, then nonequilibrium radiation transport can be of importance as is the case for AOTV applications.[1]

The Navier-Stokes equations of continuum gas dynamics fail when the gradients of the macroscopic variables become so steep that their length scale is of the same order as the average distance traveled between collisions[2] or mean free path. Also, the Navier-Stokes equations do not form a determinate set unless the shear stresses, heat flux, and mass transfer can be expressed in terms of other macroscopic quantities. A failure to meet this relationship places a limit on the range of validity of the continuum equations. An accepted procedure for extending the limits of the continuum equations into the transitional regime is the incorporation of slip boundary conditions,[3] which provide improved agreement[4] between calculated and measured surface quantities.

Computationally, there appears to be no alternative to the particle approach when the local Knudsen number is of order unity and higher.[5] Consequently, Monte Carlo (any method that employs random numbers) procedures have been developed over the past twenty-five years to provide a numerical simulation capability within the transitional flow regime. Of the various techniques for the Monte Carlo simulation of gas flows, the direct simulation Monte Carlo (DSMC) method is the one most readily applied to complex problems.[6] In the current study, the DSMC method as developed by Bird[2,7] is used to calculate the flow about blunt wedges with small body half-angles. The calculations are for the transitional regime; that is, the region bounded by continuum and free-molecule flow. The computational code is identical to that used in Refs. 8 and 9 to calculate the flow along the windward surface of the Shuttle Orbiter nose during re-entry.

In an effort to obtain further insight into the nature of the flow and the aerothermodynamic characteristics of blunt wedges under hypersonic transitional flow conditions, a numerical study was made of the flow about wedges, with body half-angles of 0, 5, and 10 deg. The altitude range considered was 70 to 100 km where the freestream velocity was assumed constant at 7.5 km/s. The calculations account directly for translational, rotational, vibrational, and chemical nonequilibrium effects where a five-species gas model is utilized. This paper emphasizes the sensitivity of both the surface quantities and the flowfield structure to variations in rarefaction and the effect of the expansion downstream of the stagnation region on the flow. Of particular interest is the identification of the flow conditions where the onset of chemical reactions occurs and the magnitude of the velocity slip and temperature jump.

The Direct Simulation Monte Carlo Method

In the DSMC method, the intermolecular collisions are considered on a probabilistic rather than a deterministic basis. Furthermore, the real gas is modeled by some thousands of simulated molecules in a computer. The velocity components, internal states, and position coordinates of these molecules are stored in the computer and are modified with time as the molecules are concurrently followed through representative collisions and boundary interactions in simulated physical space. The time parameter in the simulation may be identified with physical time in the real flow, and all calculations are unsteady. When the boundary conditions are such that the flow is steady, then the solution is the asymptotic limit of the unsteady flow. The computation is always started from an initial state that permits an exact specification such as a vacuum or uniform equilibrium flow. Consequently, the method does not require an initial approximation to the flowfield and does not involve any iterative procedures. A computational cell network is required in physical space only, and then only to facilitate the choice of potential collision pairs and the sampling of the macroscopic flow properties. Furthermore, advantage may be taken of flow symmetries to reduce the dimensions of the cell network and the number of position coordinates that need be stored for each molecule, but the collisions are always treated as three-dimensional phenomena. The boundary conditions are specified in terms of the behavior of the individual molecules rather than the distribution function. All procedures may be specified in such a manner that the computational time is directly proportional to the number of simulated molecules.

A more detailed discussion of the "variable hard sphere" (VHS) molecular model, the recommended model for the simulation of gases in an engineering context, is given in Ref. 7. Of particular relevance is the discussion of the models that account for internal energy effects and chemical reactions. The VHS model and the reactive cross sections used in the present Monte Carlo simulations are the same as those used in Ref. 9 for simulating the external flow about the Shuttle Orbiter nose.

Conditions for Calculations

Five sets of freestream conditions corresponding to altitudes ranging from 70 to 100 km are used for the present DSMC calculations. The conditions along with selected results are summarized in Table 1. For altitudes of 90 km and above, the freestream conditions are those given by Jacchia[10] for an exospheric temperature of 1200 K, whereas the conditions below 90 km are those given by Ref. 11. For the present study, the freestream velocity and wall temperature are assumed constant at 7.5 km/s and 1000 K, respectively. Also, the wall is assumed to be diffuse with full thermal accommodation and to promote the recombination of the oxygen and nitrogen

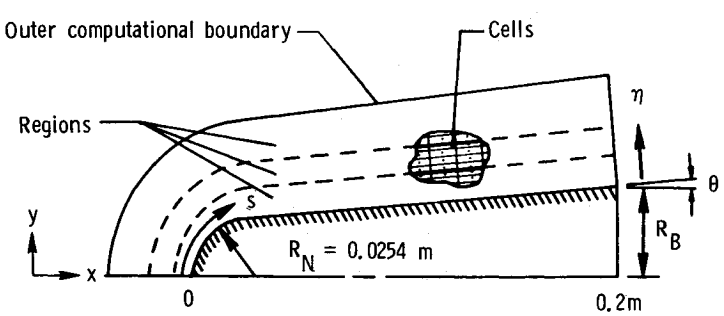

Fig. 1 Computational domain for plane configurations.

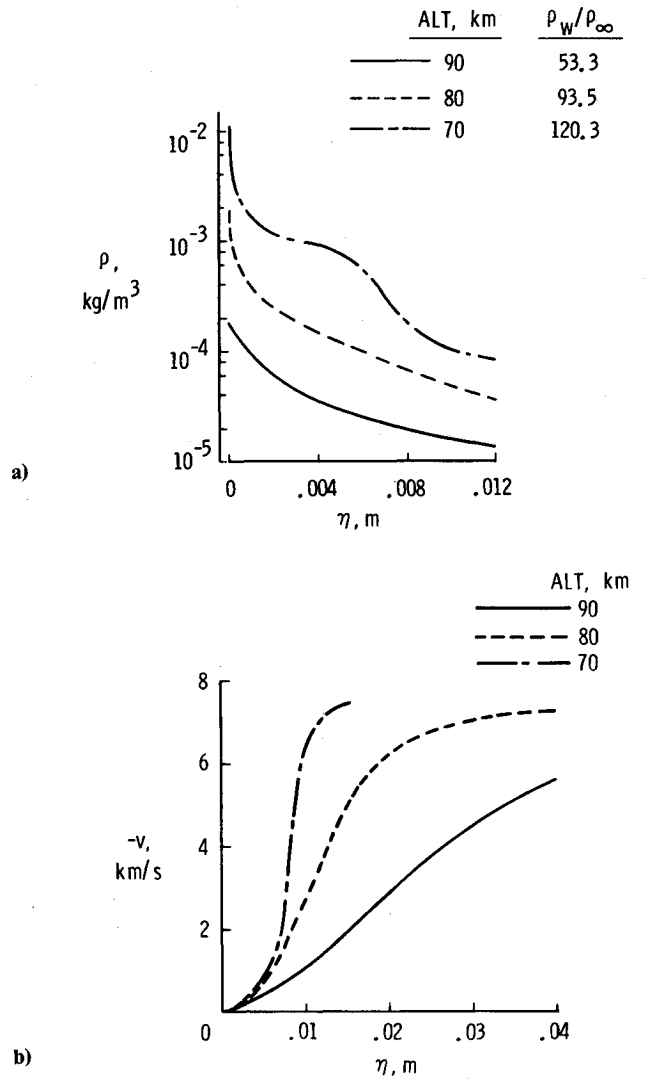

Fig. 2 Effect of rarefaction on stagnation streamline values: a) density profiles, b) normal velocity profiles.

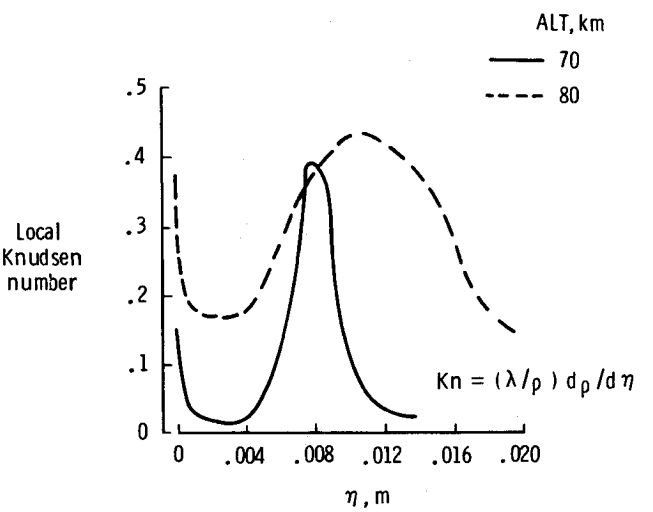

Fig. 3 Local Knudsen number values along the stagnation streamline.

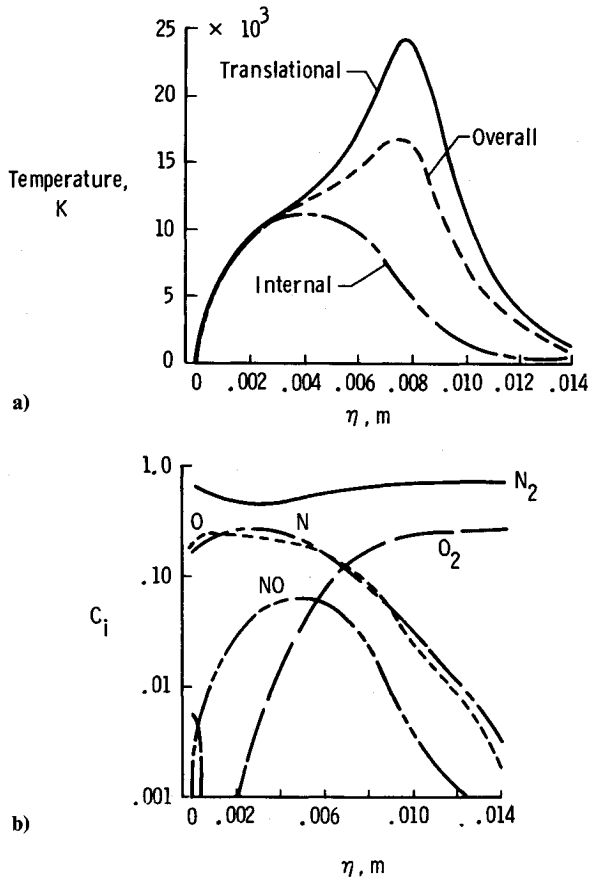

Fig. 4 Flowfield structure along the stagnation streamline (Alt = 80 km): a) extent of thermodynamic nonequilibrium, b) species mass fractions.

atoms. Recombination probabilities appropriate for the Shuttle thermal protection tiles are imposed. The oxygen[12] and nitrogen[13] recombination probabilities are 0.0049 and 0.0077, respectively. Several freestream parameters that are often used to characterize a flowfield are included in Table 1b.

The present DSMC calculations use the sample chemical kinetics model as Ref. 14 (the species O, O_2, N, N_2, and NO with 35 chemical reactions). However, the rate constants have been converted to reaction cross sections.

A view of the computational domain is depicted in Fig. 1. This domain consists of one or more arbitrary regions within which the time step and the weighting factor that relate the number of computational molecules to the number of physical molecules are constants. The smallest unit of physical space is the cell, which provides a convenient reference for the sampling of the macroscopic gas properties. The dimensions of the cells must be such that the change in flow properties across each cell is small. Time is advanced in discrete steps such that each step is small in comparison with the mean collision time.

For a given body, the computational requirements increase significantly with increasing freestream density since both the time step and cell size must be reduced, yet some minimum number of computational molecules per cell must be maintained. Because of the rather long run time for the 70 km condition, only the flow about the blunted nose is calculated.

Results and Discussion

This section will focus on the DSMC calculated results for cylindrically blunted wedges with half-angles of 0, 5, and 10 deg. Results at 70 and 85 km are emphasized to demonstrate and contrast differences in the flow structure corresponding to near continuum and significantly rarefied conditions, respectively.

Two fundamental quantities for gas dynamic flows are number density and velocity, quantities that are neither in-

Table 1 Conditions and results

a) Freestream conditions

Altitude, km	Density, kg/m^3	U_∞, km/s	T_∞, K	Mole fractions X_{O_2}	X_{N_2}	X_O	$\bar{M}$, g/mol	λ_∞, m
100	5.641×10^{-7}	7.5	194	0.177	0.784	0.039	28.26	1.37×10^{-1}
95	1.396×10^{-6}	7.5	189	0.197	0.787	0.016	28.61	5.59×10^{-2}
90	3.418×10^{-6}	7.5	188	0.209	0.788	0.003	28.81	2.30×10^{-2}
85	7.955×10^{-6}	7.5	181	0.237	0.763	0	28.96	9.94×10^{-3}
80	1.999×10^{-5}	7.5	181	0.237	0.763	0	28.96	3.96×10^{-3}
70	8.753×10^{-5}	7.5	220	0.237	0.763	0	28.96	9.03×10^{-4}

b) Various parameters and results

Altitude, km	Re_∞	Kn_∞	K_r^2	S_∞	Stagnation heat flux, kW/m^2	C_D Plate	C_D Wedge[a]	$C_{F,\max}$
100	8	5.38	0.05	22.2	102	1.29	1.01	0.795
95	21	2.20	0.11	22.6	235	1.29	–	0.683
90	52	0.91	0.28	22.8	511	1.22	0.85	0.555
85	125	0.39	0.64	23.3	928	1.07	0.73	0.385
80	313	0.16	1.61	23.3	1451	0.90	0.61	0.229
70	1159	0.04	7.05	21.1	1920	–	–	–

[a] $\theta = 5$ deg.

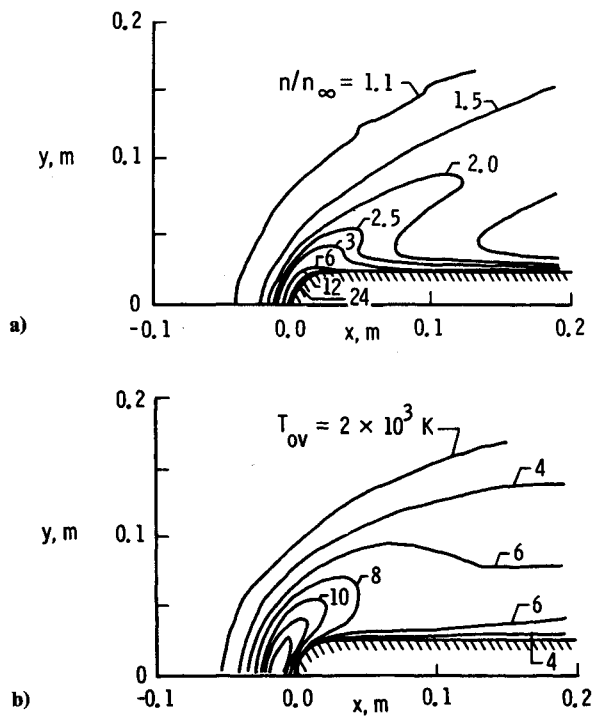

Fig. 5 Flowfield contours (Alt = 85 km): a) number density ($n_\infty = 1.65\times10^{20}$m^{-3}), b) overall kinetic temperature.

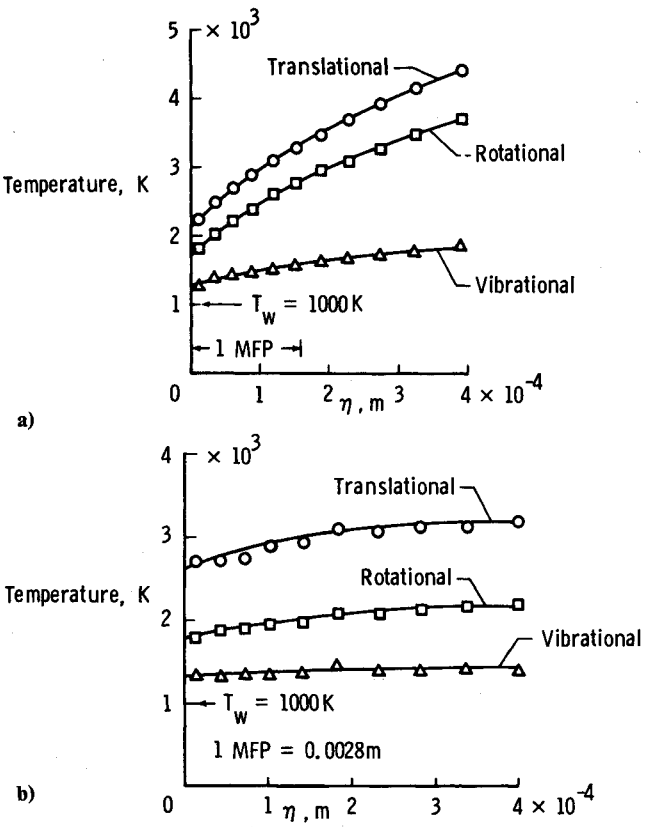

Fig. 6 Kinetic temperatures adjacent to the wall (Alt = 85 km): a) $s/R_N = 0$, b) $s/R_N = 4.1$.

ferred nor dependent on the condition of thermal equilibrium, such as is the case for temperature and pressure. The variation of density and velocity along the stagnation streamline and their dependence on rarefaction is demonstrated in Fig. 2 for altitudes of 70 and 90 km. (Please note that for Fig. 2 and subsequent figures, the results for the complete extent of the computational domain may not be shown, in an effort to emphasize points of interest.) Two regions of interest are those near the wall and the shock wave. Near the wall, a large increase in density occurs which is characteristic of cold-wall reentry conditions. At 70 km, the stagnation density is more than two orders of magnitude greater than the freestream value. As for the shock wave, the calculated results show a continuous shock wave structure even for the lowest altitude case. For the 70 km condition, there is an inflection in the density profile, which would obviously become more pronounced

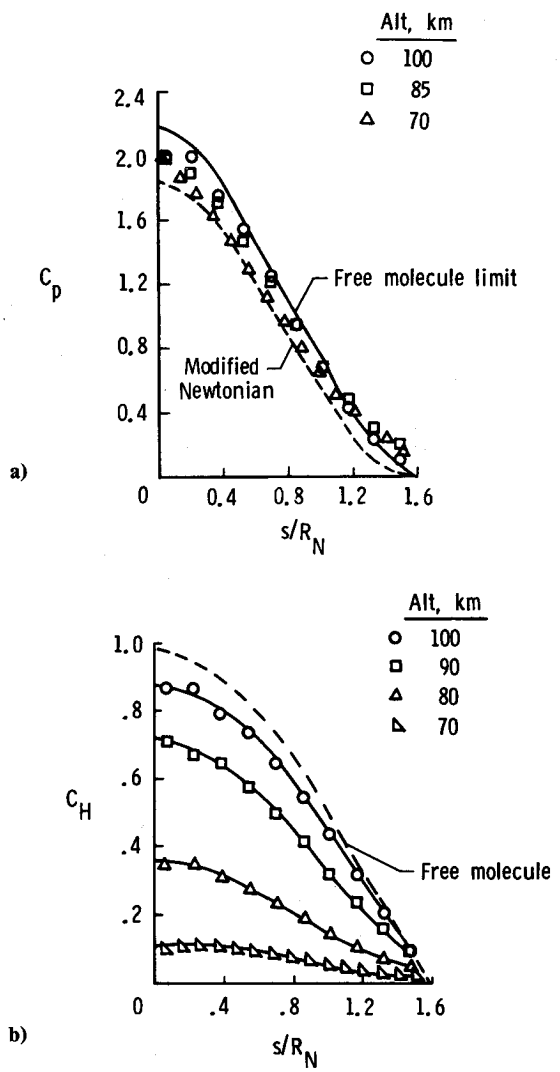

Fig. 7 Effect of rarefaction on wall quantities: a) pressure coefficient, b) heat transfer coefficient.

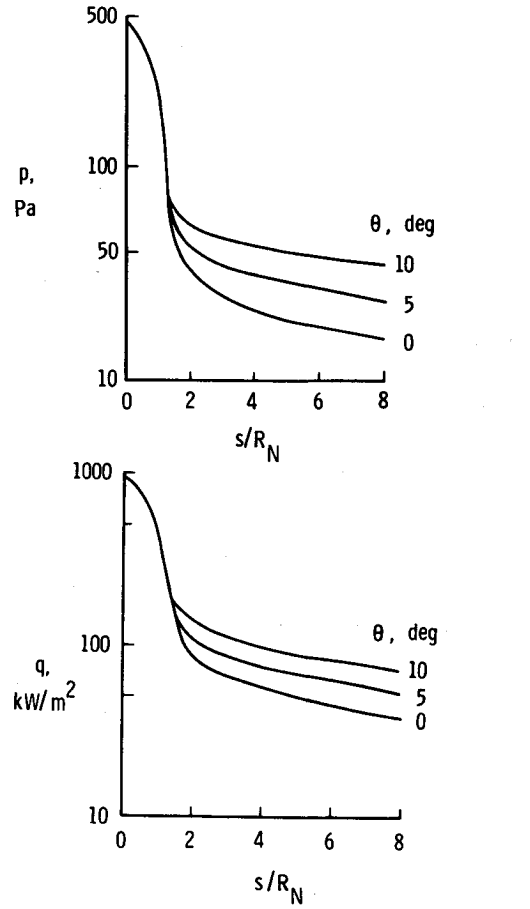

Fig. 8 Effect of wedge angle on wall quantities (Alt = 85 km): a) pressure distribution, b) heat transfer rate distribution.

for less rarefied conditions. Even so, the shock wave thickness for the 70 km case is of the same order of thickness as the shock layer. The normal velocity profiles (Fig. 2b), which approach the freestream velocity of 7.5 km/s, also show a more gradual merging of the shock layer and shock wave with increasing rarefaction. As a point of reference, the Rankine-Hugonoit relations give a postshock velocity of 0.75 km/s, which corresponds to a small fraction of the total flowfield disturbance as predicted by the DSMC method.

The degree of rarefaction of a low-density flow is usually expressed in terms of an overall Knudsen number as is listed in Table 1 for the present flow conditions. The overall Knudsen number is defined as the ratio of the molecular mean free path in the freestream gas to a characteristic dimension of the flowfield, such as the nose radius or body diameter. The larger the Knudsen number, the more rarefied the flow. The overall Knudsen number has and will continue to serve as a useful parameter in correlating data, but it must be used with caution when assessing where rarefaction effects are important. The problem with the overall Knudsen number characterization is readily evident for a slender body, where the density downstream of the stagnation region may be fifty times smaller than the stagnation point value, as is the case for some of the present calculations. Furthermore, such a characterization does not account for variations in surface conditions or shock wave strength (extent of bluntness). Obviously, a more realistic

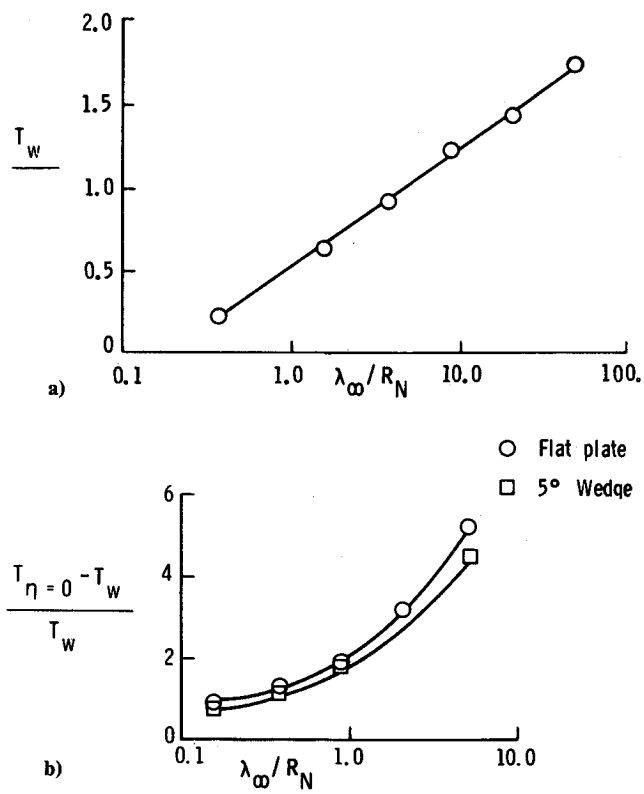

Fig. 9 Effect of rarefaction on temperature jump: a) $s/R_N = 0$, b) $s/R_N = 4.1$.

description would be a Knudsen number that is indicative of the local conditions within the flowfield as has been discussed by Bird.[15] For the local Knudsen number, the characteristic length is defined in terms of the gradient of a macroscopic property such as density. Therefore, the larger the gradient becomes with respect to the local mean free path, the more rarefied the flow.

The variation of the local Knudsen number along the stagnation streamline is shown in Fig. 3 for the 70 and 80 km cases. Significant variations are evident, with the value being generally larger near the surface and in the shock wave. A suggested[15] rule of thumb is that the continuum equations should not be used when the local Knudsen number exceeds a critical value of about 0.2 to 0.3. According to this criterion, a significant amount of the stagnation region flow for the 80 km case would be inappropriately modeled using a continuum description. Also, as was cited in Ref. 15, the fractional temperature jump at the wall (see Fig. 9a) is of the same order as the Knudsen number adjacent to the wall for the two-dimensional stagnation calculations.

The stagnation temperature and species mass fraction profiles for the 70 km case are presented in Figs. 4a and 4b, respectively. Thermodynamic nonequilibrium is evident throughout the shock wave and into the outer part of the shock layer, as evidenced by the lack of equilibration of the translational and internal kinetic temperatures. The overall kinetic temperature shown is defined for a nonequilibrium gas as the weighted mean of the translational and internal temperature (see Eq. 1.26 of Ref. 2). Note that the ideal gas equation of state does not apply to this temperature in a nonequilibrium situation. Only under thermal equilibrium conditions is the overall kinetic temperature and the thermodynamic temperature equivalent.

The translational kinetic temperature rise, which is quite rapid, always precedes the density rise (Fig. 2a). For example, the translational kinetic temperature is maximum at 7.84 cm from the surface while the density has increased by only a factor of 2.1. The initial translational kinetic temperature rise results from the essentially bimodal velocity distribution, the molecular sample consisting of mostly undisturbed freestream molecules with just a few molecules that have been affected by the shock. The large velocity separation between these two classes of molecules gives rise to the early translational kinetic temperatures (two counterflowing streams of molecules under collisionless conditions would produce a translational kinetic temperature). The collisions that do occur in the outer portion of the shock wave are highly energetic, and much of the chemical change occurs within the shock wave (Fig. 4b).

As the flow becomes more rarefied, the extent of the flowfield disturbances becomes much larger, as evidenced by the number density and temperature contours shown in Fig. 5 for flow about a blunted flat plate at a 85-km altitude. For example, the overall kinetic temperature disturbance extends about 2.5 nose radii upstream of the surface in the stagnation region (Fig. 5b) and more than 6 nose radii away from the surface at an s/R_N location of 8. The conditions along the surface experience significant change with the expansion to the downstream conditions: the stagnation density is seventy-five times freestream (not shown in Fig. 5a since the density in-

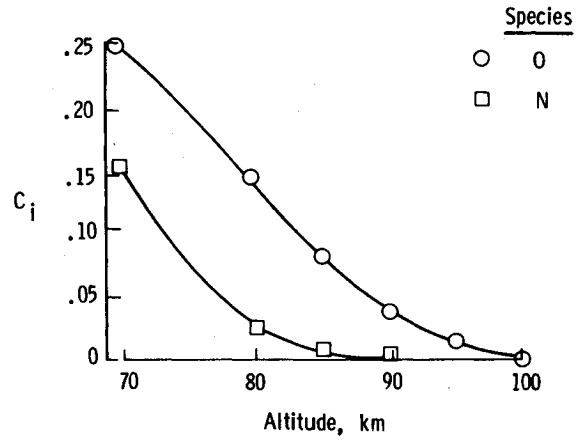

Fig. 11 Maximum atomic mass fraction values along the stagnation streamline.

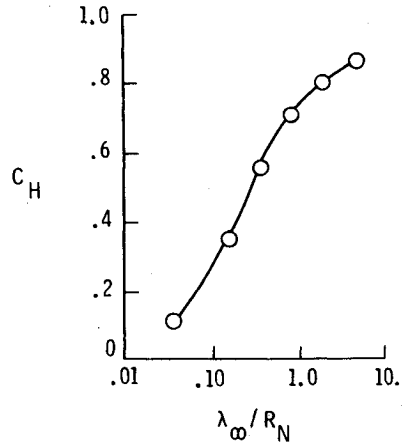

Fig. 12 Stagnation point heat transfer coefficient vs Knudsen number ($s/R_N = 0$).

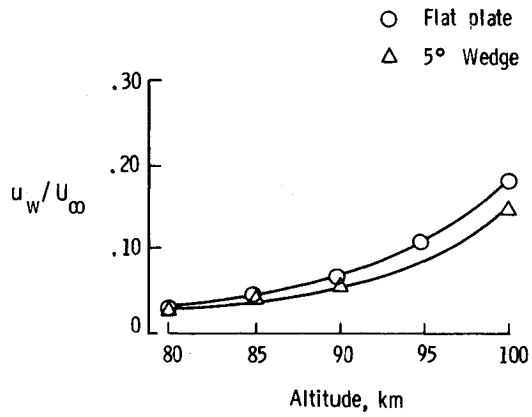

Fig. 10 Effect of rarefaction on velocity slip ($s/R_N = 4.1$).

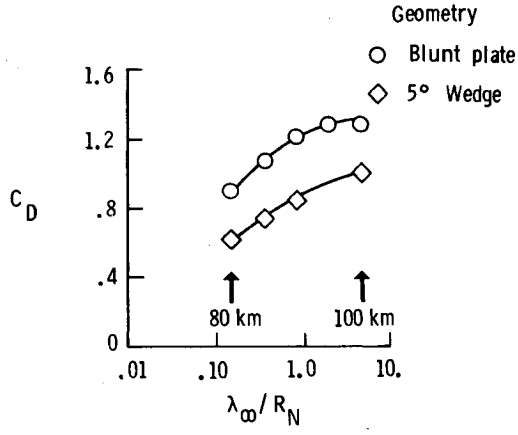

Fig. 13 Drag coefficient vs Knudsen number.

creases substantially near the surface), whereas the surface density near the end of the plate is only three times freestream.

Even though the gas is significantly compressed in the stagnation region, the kinetic temperature profiles along the stagnation streamline and near the surface (Fig. 6a) show that thermodynamic equilibrium is not achieved; that is, the energy associated with the translational and internal energy modes does not conform to a Boltzmann distribution. Furthermore, the overall kinetic temperature of the gas adjacent to the surface is 1920 K, almost twice the specified wall temperature. At a distance of about one local mean free path (MFP) from the surface, the overall kinetic temperature is 3300 K, the value specified as the jump condition in continuum formulations.[3] The temperature jump values are even greater at an s/R_N location of 4.1 (Fig. 6b), where the overall kinetic temperature adjacent to the surface is 2252 K.

Surface Pressure and Heat Transfer

Surface pressure and heat transfer values expressed in coefficient form are presented in Figs. 7a and 7b, respectively, for the cylindrically blunted portion of the flat plate. The effects of rarefaction are demonstrated by comparing the calculated results for 70, 85, and 100 km. The pressure coefficient data are bounded by the modified Newtonian and free molecule values for most of the nose region. The variation of the pressure coefficient caused by rarefaction effects is moderate provided that the gas surface interaction is diffuse, as is assumed in the present calculations. In contrast, the heat transfer coefficient (Fig. 7b) is very sensitive to rarefaction effects, approaching the free molecule value with increasing rarefaction.

Effect of Wedge Angle

For the 85-km condition, calculations were made for wedge half-angles of 0, 5, and 10 deg. Results for pressure and heat transfer rate distribution are shown in Figs. 8a and 8b, respectively. The qualitative trends for pressure and heat transfer rate distributions are as expected. Note, however, that the calculated pressure aft of the nose is higher than either Newtonian or free molecule. For the 10 deg wedge, the pressure at $s/R_N = 8$ is a factor of 2.6 greater than Newtonian, whereas at the nose wedge juncture, it is 5.2 times Newtonian.

Temperature Jump and Wall Slip

Figure 9 presents the values of temperature jump for a 5 deg wedge and the flat plate as a function of the freestream Knudsen number. The results at the stagnation point, where both cases are identical (Fig. 9a), and an $s/R_N = 4.1$ (Fig. 9b) show the jump values to be larger on the afterbody section. The effect of the body half-angle is small on the jump condition in the afterbody section, and a similar trend is found for the velocity slip as shown in Fig. 10.

The extent of the flowfield disturbance is significantly different for the various altitudes studied; this will have important implications concerning the gas-phase chemistry and the importance of the gas-surface catalytic activity. An indication of this effect is presented in Fig. 11, where the maximum value of atomic mass fractions along the stagnation streamline are shown as a function of altitude for both the monoatomic nitrogen and oxygen species. The onset (atomic mass fraction exceeds 1%) of oxygen dissociation occurs at about 96 km and at about 90 km for nitrogen.

Heating and Drag Coefficients

The stagnation point heat transfer coefficient as a function of the freestream Knudsen number is presented in Fig. 12 for both the 5 deg wedge and the flat plate. Qualitatively, the results are what one would expect, increasing from the small value near the continuum regime to a value of unity as the free molecule limit is approached.

As for the drag coefficient, Fig. 13 shows the calculated data for the plate and the 5 deg wedge as a function of the freestream Knudsen number. As with the heat transfer coefficient, the drag coefficient experiences a large increase with increasing rarefaction. The change in drag is due primarily to the increase in skin friction rather than to a change in the pressure coefficient. The difference between the two curves is due primarily to the difference in base area, since the drag force for the 5 deg wedge is only 10% greater than that for the flat plate.

Concluding Remarks

Through the use of a DSMC method, the flowfield structure and surface quantities about blunt wedges have been calculated for re-entry conditions within the transition flow regime. Results of the calculations show the following:

1) The calculated onset of dissociation occurs at 96 km.

2) Translational and thermodynamic nonequilibrium occurs throughout most of the body-influenced flowfield for the flow conditions studied.

3) Calculated surface temperature jump and velocity slip are significant for the conditions investigated.

The numerical results presented herein focus on the nonequilibrium aspects of rarefied hypersonic flows. Comparisons of data calculated with a particulate and a continuum method illustrate many of the possible deficiencies in the application of continuum methods for re-entry transitional flows. Even though the particulate approach is computationally demanding in terms of resources, it does provide a means of simulating the physics of real-gas flows. Yet a major problem is the lack of reliable experimental data that can be used to either verify or provide the basis for improving the methods. Therefore, inflight measurements of flowfield composition and profile quantities are urgently needed. This is particularly true since no amount of simulation will, by itself, provide basic physical information. Yet simulation methods can provide information on flows that are not amenable to analysis and for which experiment is either impractical or impossible.

References

[1]Howe, J.T., "Introductory Aerothermodynamics of Advanced Space Transportation Systems," AIAA Paper 83-0406, Jan. 1983.

[2]Bird, G. A., *Molecular Gas Dynamics,* Clarendon Press, Oxford, 1976.

[3]Gupta, R. N., Scott, C. D., and Moss, J. N., "Slip-Boundary Equations for Multicomponent Nonequilibrium Airflow," NASA TP-2452, Nov. 1985.

[4]Boylan, D. A., "Laminar Convective Heat-Transfer Rates on a Hemisphere Cylinder in Rarefied Hypersonic Flow, "*AIAA Journal,* Vol. 9, Aug. 1971, pp. 1661-1663.

[5]Bird, G. A., "Monte Carlo Simulation of Gas Flows," *Annual Reviews of Fluid Mechanics,* Vol. 10, edited by M. D. Van Dyke et al., Annual Reviews Inc., Palo Alto, CA, 1979, p. 11.

[6]Bird, G. A., "Simulation of Multi-Dimensional and Chemically Reacting Flows," *Rarefied Gas Dynamics,* Vol. 1, CEA, Paris, 1979.

[7]Bird, G. A., "Monte Carlo Simulation in an Engineering Context," *AIAA Progress in Astronautics and Aeronautics: Rarefied Gas Dynamics,* Vol 74, Part 1, edited by Sam S. Fisher, 1981, pp. 239-255.

[8]Moss, J. N. and Bird, G. A., "Direct Simulation of Transitional Flow for Hypersonic Re-entry Conditions," *Progress in Astronautics and Aeronautics: Thermal Design of Aeroassisted Orbital Transfer Vehicles,* edited by H. F. Nelson, Vol. 96, 1985, pp. 113-139.

[9]Moss, J. N. and Bird, G. A., "Monte Carlo Simulations in Support of the Shuttle Upper Atmospheric Mass Spectrometer Experiment," AIAA Paper 85-0968, June 1985.

[10]Jacchia, L. C., "Thermospheric Temperature, Density, and Composition: New Models," *Research in Space Science,* SAO Special Report 375, March 1977.

[11]*U. S. Standard Atmosphere,* 1962.

[12]Zoby, E. V., Gupta, R. N., and Simmonds, A. L., "Temperature-Dependent Reaction Rate Expressions for Oxygen," *Progress in Astronautics and Aeronautics: Thermal Design of Aeroassisted Orbital Transfer Vehicles,* edited by H. F. Nelson, Vol. 96, 1985, pp. 445-464.

[13]Scott, C. D., "Catalytic Recombination of Oxygen and Nitrogen in High Temperature Reusable Surface Insulation," *Progress in Astronautics and Aeronautics: Aerothermodynamics and Planetary Entry,* edited by A. L. Crosbie, Vol. 77, 1981, pp. 192-212.

[14]Shinn, J. L., Moss, J. N., and Simmonds, A. L., "Viscous Shock-Layer Analysis for the Shuttle Windward Symmetry Plane with Surface Finite Catalytic Recombination Rates," *Progress in Astronautics and Aeronautics: Entry Vehicle Heating and Thermal Protection Systems,* edited by Bauer and Collicott, Vol. 85, 1983, pp. 149-180.

[15]Bird, G. A., "Low-Density Aerothermodynamics," *Progress in Astronautics and Aeronautics: Thermophysical Aspects of Re-Entry Flows,* edited by J.D. Moss and C.D. Scott, Vol. 103, 1986, pp. 3-24.